ACCESS TO EDGE TRANSPORT BARRIERS AND PROJECTIONS OF PEDESTAL PERFORMANCE IN THE SPARC TOKAMAK

J.W. HUGHES
MIT Plasma Science and Fusion Center
Cambridge, Massachusetts, United States
Email: jwhughes@psfc.mit.edu

A.E. HUBBARD, P. RODRIGUEZ-FERNANDEZ, T.M. WILKS, N.T. HOWARD
MIT Plasma Science and Fusion Center
Cambridge, Massachusetts, United States

D.J. BATTAGLIA, A.J. CREELY
Commonwealth Fusion Systems
Devens, Massachusetts, United States

Abstract

Access to a sufficiently large edge pedestal on the SPARC tokamak will be a key ingredient in the realization of high fusion gain on this compact (R=1.85m, a=0.57m) high field (reference BT=12.2T) device. Following initial investigations of access to H-mode operation and predictions for pedestal pressure in the SPARC Primary Reference Discharge (PRD), projections of I-mode access have been made, with the aim of identifying potential scenarios of high confinement operation free of large edge localized modes (ELMs). Power threshold projections for the I-mode regime are comparable to those for H-mode, and in the highest B_T scenarios, potentially less demanding. Initial investigations to map I-mode pedestals from existing devices on SPARC show promise for utilizing the regime to remain away from H-mode and large ELMs.

1. INTRODUCTION

SPARC is a medium scale (R=1.85m, a=0.57m) high field/current (B_T up to 12.2T, I_P up to 8.7MA) tokamak being built to produce net energy from DT fusion [1,2]. The design of the device incorporates high temperature superconductor (HTS) coils for the sustainment of high toroidal field, ion cyclotron range-of-frequencies (ICRF) auxiliary heating, and tungsten plasma facing components (PFCs) in the main chamber and divertor. A significant performance goal for SPARC is the demonstration of fusion gain $Q_{fus}>2$, with $Q_{fus}=P_{fus}/P_{in}$, *i.e.* the ratio of total fusion power to the input power absorbed in the plasma.

Several operational scenarios are under consideration for their potential to meet or exceed the $Q_{fus}=2$ metric. L-mode is the most straightforward scenario to achieve, requiring only successful deposition of auxiliary power. H-mode should also be achievable if available power exceeds the L-H threshold specific to SPARC. Previous work evaluated the power requirements to access H-mode under anticipated operational parameters [3], using L-H power thresholds P_{L-H} assessed with scaling laws validated on multiple existing devices [4—6]. Access to H-mode was found feasible and it was shown that a fully developed H-mode with an edge pedestal gave satisfactory performance in the SPARC Primary Reference Discharge (PRD), a full-field, full-current plasma with confinement properties extrapolated from H-modes on present day tokamaks [2,7]. Using both plasma operational contour (POPCON) frameworks and predictive integrated modelling, fusion gain well in excess of stated goals was projected.

The present work extends these considerations to the I-mode confinement regime [8]. I-mode enhances energy confinement relative to L-mode via an edge pressure pedestal, though without the formation of a significant density pedestal. Particle and impurity transport are significant in I-mode, allowing the avoidance of unwanted core density and radiated power rise, and without the presence of large edge localized modes (ELMs). The regime is a promising alternative to L-mode and H-mode for delivering the $Q_{fus}>2$ mission of SPARC, and potentially for extension to future burning plasma devices. On existing devices, I-mode is usually obtained by operating in single null plasmas with $B\times\nabla B$ directed away from the active the X-point. This tends to open a gap between the power thresholds for I-mode and H-mode, which is especially significant for high field tokamaks [9]. This paper will show the potential for this window to exist in SPARC. We will consider both simple extrapolations in total power

threshold, and also potential enhancements to access to H-mode and I-mode brought on by a significant ion heat flow in the tokamak boundary.

2. ACCESS TO CONFINEMENT BEYOND L-MODE

While L-mode performance on SPARC should be trivially obtained with application of auxiliary power, formation of an edge pressure pedestal and access to higher confinement is expected to come with minimum power requirements. This section will summarize best available projections for H-mode and I-mode access on SPARC, based on existing experience.

2.1. H-mode

Typical projections for L-H on SPARC use an adaptation of the ITPA H-mode power threshold scaling [4] that attempts to account for isotope effects:

$$P_{L\text{-}H} = 0.0488\, n^{0.72}\, B_T^{0.80}\, S^{0.94}\, (2/A_{eff}) \qquad (1)$$

with the power threshold $P_{L\text{-}H}$ in MW, line-averaged density n in $10^{20}m^{-3}$, B_T in T, boundary surface area S in m^2. A_{eff} is the effective main ion mass, 2 for D plasmas, 2.5 for a 50:50 DT mix. To account for elevated power threshold in the low density branch (LDB), an escalator is placed on this expression for density values $n<n_{th,min}$, where $n_{th,min}$ is calculated according to Equation (3) in [5] and is approximately $1.9x10^{20}m^{-3}$ for SPARC at 12.2T, 8.7MA. This $P_{L\text{-}H}$ expression is used for SPARC operational scenarios that are either double null (DN) or single null (SN) with B×∇B directed toward the active X-point. For SN plasmas with oppositely directed B×∇B, a doubling of $P_{L\text{-}H}$ is assumed. This 2x increase is based on typical tokamak experience, although there is not a commonly accepted scaling for the precise value of the $P_{L\text{-}H}$ increase.

Alternately, the power threshold may be expressed as a critical ion heat flow, as determined by an analysis of combined ASDEX Upgrade (AUG) and Alcator C-Mod L-H threshold experiments [6], giving:

$$Q_{i,L\text{-}H} = 0.0325\, n^{1.05}\, B_T^{0.68}\, S^{0.93}\, (2/A_{eff}) \qquad (2)$$

with the critical ion heat $Q_{i,L\text{-}H}$ in MW and the others defined as above. This scaling is predicated on the physical picture that a critical value of ExB shear is required to access an L-H transition, and that this is strongly correlated with the edge ion temperature gradient and driven by ion heat flux. Such a mechanism may be invoked to explain the LDB of the $P_{L\text{-}H}$ on existing machines which have strong electron heating and long electron-ion equilibration times relative to confinement time when operating at low density [5].

2.2. I-mode

No multi-machine scaling exists yet for the L-I threshold power. However, evidence from existing devices [9—12] indicates that $P_{L\text{-}I}$ scales less strongly with B_T than $P_{L\text{-}H}$. This holds some promise for opening a substantial L-I-H window in high-field tokamaks, including SPARC. As with L-H, there is experimental evidence from AUG that L-I transitions occur at a critical ion heat flux which scales nearly linearly with density [11]. By assuming a scaling that is exactly linear in n and S and keeping the exponent on B_T a free parameter, we can transform the AUG result into an expression for L-I threshold:

$$Q_{i,L\text{-}I} = 0.07\, n\, (B_T/2.4)^{\alpha}\, S\, (2/A_{eff}) \qquad (3)$$

keeping for now the inverse dependence on isotope mass, even though the A_{eff} dependence may be somewhat weaker than in the case of L-H. Under conditions of equal electron and ion heat flow and neglecting radiated power, one can take $P_{L\text{-}I}=2Q_{i,L\text{-}I}$ and compare with experiment. L-I threshold data from Alcator C-Mod, previously presented in [9], are used to make example comparisons.

Fig. 1 shows two plots of P_{L-I} scalings vs. actual experimental power threshold for these data. Fig. 1a compares data to the best fit scaling determined in [9], which is linear in both n and S by design and scales with $B_T^{0.26}$. This expression performs reasonably well across the C-Mod data, which span $2.7<B_T[T]<8.0$ and $0.8<n[10^{20}m^{-3}]<2.4$ and have S of approximately $7m^2$. These same data were compared with values 2x the expression in Eq. (3), with the B_T exponent α varied over a range of 0.15 to 0.5, roughly in line with the extremes in confidence intervals noted in the AUG literature [10,11]. These AUG-inspired scalings can capture qualitatively the B_T dependence seen on C-Mod, although they predict too low a P_{L-I} on average. Fig. 1b compares a relatively well performing fit of this type, with $P_{L-I}\sim B_T^{0.39}$, with the same C-Mod data set. The experimental values fall largely between the scaling and 1.5X the scaling in this case. To further probe this, it would be desirable to directly compare the ion power flowing through the edge to Eq. (3). There is no routine experimental Q_i from C-Mod, but transport calculations of L-mode plasmas on C-Mod often find that the ion power is significantly less than half the input power (see for example [6]). A tendency for $P> 2Q_i$ could partly explain the underprediction of the scalings based on ion heat flux.

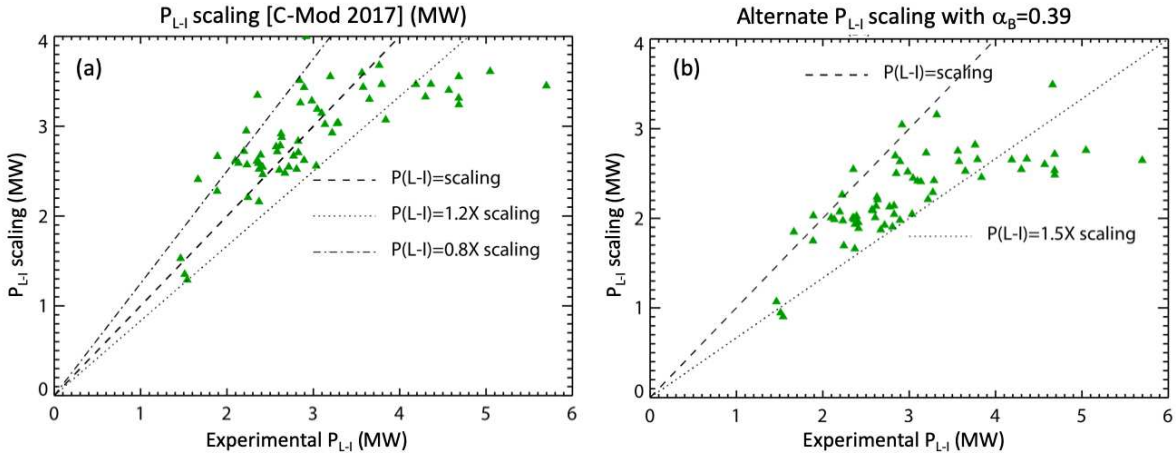

FIG. 1. Scaling expressions for the I-mode power threshold P_{L-I} compared to experimental power at L-I transitions on Alcator C-Mod. The scalings are both of the form $P\sim C\ n\ S\ B_T^{\alpha}$ and have differing lead coefficients and exponents α. (a) The scaling derived from these data and presented in [9] shows good agreement on average. (b) The scaling composed of twice the expression in (3) and with $\alpha=0.39$ trends correctly but on average underpredicts the total power at L-I threshold.

We can apply the same method to estimating the L-I threshold for SPARC. Generally the P_{L-I} projections for B×∇B opposite the X-point are quite comparable to P_{L-H} with B×∇B toward the X-point, and so, assuming the upper I-H boundary is approximately $2P_{L-H,ITPA}$, a window of feasibility exists for I-mode in SPARC SN plasmas with unfavourable drift selected. By way of example, Fig. 2 shows operational space in power and density for both 8T and 12.2T scenarios in DT plasmas. As was shown in [3], the conventional L-H power threshold curve (blue dashed dot) is reachable at power levels of ~20MW, which is approaching the maximum auxiliary power complement of 25MW. If P_{L-H} is effectively doubled in unfavourable drift, the solid blue curve would give the L-H boundary. The purple curves illustrate power thresholds for I-mode, assuming the total power requirement is twice the expression for ion heat in Eq. (3). The solid purple curve represents a field scaling of $\alpha=0.26$, which was inspired by the 2017 C-Mod scaling [9]. (Note the resulting expression is not the same as that used for the comparison in Fig. 1a. The leading coefficient is the smaller one used in Fig 1b.) The dashed curves represent $\alpha=0.15$ and $\alpha=0.49$ (extremes of confidence intervals from AUG [10,11]). These graphs illustrate the promise of opening up a L-I-H gap on SPARC, particularly at density values below about $3x10^{20}m^{-3}$. Particularly successful DT I-modes, fortified by alpha heating, could in principle approach the nominal H-mode power threshold (red curve).

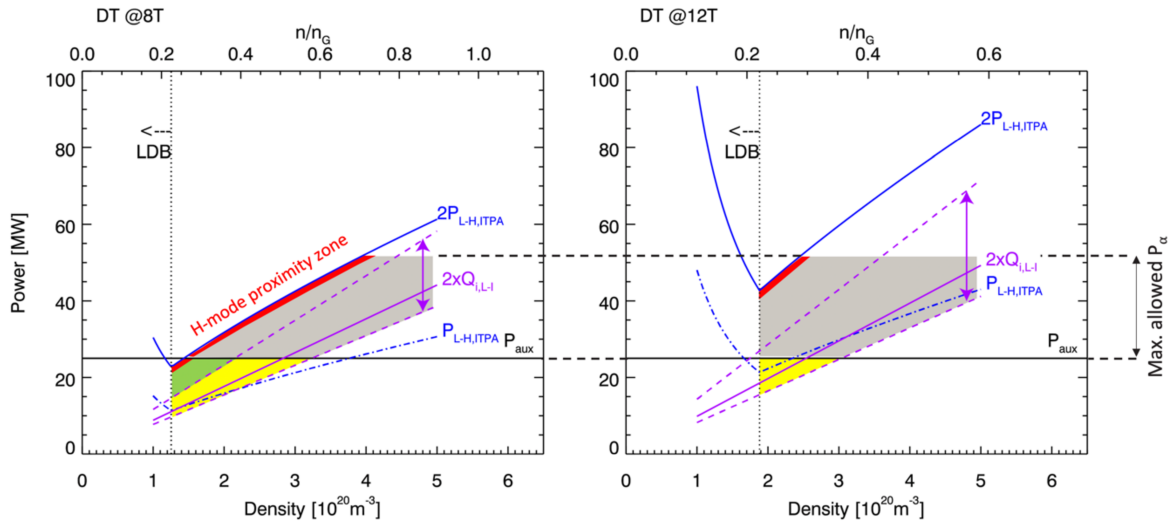

FIG. 2. Power/density operational space in DT SPARC plasmas at 8T, 5.7MA and at 12.2T, 8.7MA. The isotope and density adjusted ITPA $P_{L\text{-}H}$ (blue dashed) is similar in magnitude to the simplified $P_{L\text{-}I}$ projections (purple), near the anticipated L-mode operating densities (n/n_G~0.2). $P_{L\text{-}H}$ is assumed to double in unfavourable drift cases (blue solid), opening a window of I-mode operation. Yellow regions show promise for I-mode access with up to 25MW of auxiliary RF power, the green region looks highly favourable, and grey regions require additional power from alpha heating.

Under the assumptions presented above, the I-mode windows become smaller in DD scenarios, but remain finite and attractive for potential pre-DT exploration. This is illustrated in Fig. 3. A key question for both DD and DT scenarios is the behaviour of Q_i and its impact on $P_{L\text{-}I}$ at low density.

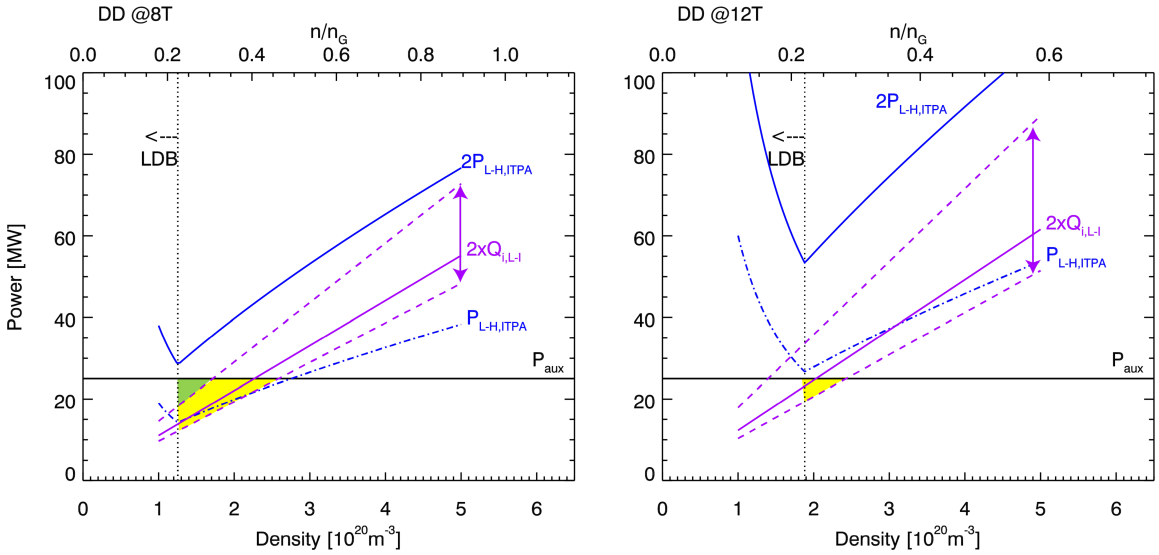

FIG. 3. Power/density operational space in DD SPARC plasmas at 8T, 5.7MA and at 12.2T, 8.7MA. Colour coding is as in Fig. 2.

3. PROXIMITY TO CONFINEMENT TRANSITIONS IN SPARC L-MODES

The SPARC core plasma has been modelled to assess its fusion performance, both in the PRD scenario and in cases with reduced fusion gain. Initial operations are likely to occur at input power significantly less than the maximum RF input of 25MW. Inspection of Figs. 2,3 clearly shows these scenarios may be marginal to H-mode and I-mode access. L-mode simulations have been performed using PORTALS [13], a framework capable of predicting the multichannel (T_e, T_i, n_e) core profiles (in this case, $\rho_\phi < 0.9$) with nonlinear CGYRO and self-

consistent energy exchange, alpha heating and radiation. These simulations provide P_{NET}, the net power transported across flux surfaces calculated at $\rho_\phi = 0.95$, and also the balance of power flow in the ion and electron channels $Q_i+Q_e=P_{NET}$. Since there are localized heat losses (*e.g.* radiation, charge exchange) in the outer 5% of the plasma minor radius, these numbers represent an upper bound on the amount of power flowing across the separatrix. Table 1 shows outputs from initial L-mode simulations scanning RF power and density. Several power balance quantities are given, along with the H-factor computed from the simulation. Here H_{97} is the ratio of energy confinement time to the 1997 L-mode confinement scaling [14]. Note that H_{97} is an output of the simulation, rather than an input. In order to achieve a range of computed energy confinement in the simulation, the input edge temperature has been varied. The list in Table 1 has been filtered to include only cases with H_{97} near unity, as one would expect in an L-mode tokamak.

TABLE 1. Results of six L-mode simulations of SPARC DT plasmas at 12.2T, 8.7MA. Scanned inputs include RF power, density and edge temperature (effectively varying the H-factor). P_{NET}/P_{L-H} is evaluated using Eq. (1), $Q_i/Q_{i,L-H}$ uses Eq. (2), and $Q_i/Q_{i,L-I}$ uses Eq. (3) with a=0.26. The rows in bold demonstrate potential access to H-mode and/or I-mode, based on the ratios in the last two columns

RF[MW]	n_{20}	H_{97}	P_{NET}[MW]	Q_i/P_{NET}	P_{NET}/P_{L-H}	$Q_i/Q_{i,L-H}$	$Q_i/Q_{i,L-I}$
5.0	**1.0**	**0.88**	**7.3**	**0.69**	**0.56**	**0.83**	**1.04**
5.0	2.1	0.80	2.9	0.81	0.13	0.17	0.22
14.9	**1.0**	**1.03**	**17.5**	**0.66**	**1.31**	**1.85**	**2.31**
14.9	**1.4**	**0.96**	**16.7**	**0.72**	**0.99**	**1.36**	**1.73**
14.9	**1.4**	**1.16**	**17.1**	**0.73**	**0.99**	**1.38**	**1.76**
14.9	2.2	0.89	13.0	0.74	0.54	0.66	0.85

The SPARC core is found to have well equilibrated electrons and ions and has stiff profiles as it is dominated by ITG turbulence. Significant power deposition occurs on ions from RF heating, and the electron channel experiences strong losses from radiation. One outcome of these features appears to be that, unlike most present wave-heated devices, SPARC has a relatively large ratio of ion to electron heat flux at the edge, expressed as Q_i/Q_e. All cases have an ion heat flow fraction $Q_i/P_{NET}>0.5$, despite most of the points being below the LDB density predicted by the formulation in [6]. In a number of low to modestly powered L-modes, the resulting ion heat flows can approach the projections for L-H and L-I access, and these are indicated in Table 1 by bold type. This result holds considerable promise for access to increased energy confinement states at reduced input power. Additional simulations are planned across a range of density and power to help guide development of L-mode scenarios, and to seek operational routes to confinement transitions. Prediction of edge temperature in L-modes has high leverage on the results and requires further study. Further work will also be needed to assess the compatibility of these simulated cases with the power handling capabilities and projected sputtering rates in the SPARC divertor.

4. PEDESTAL PROJECTIONS

Predictions of the realized pedestal in H-mode have been performed using the EPED model [15]. Over the range of feasible densities in SPARC, the H-mode pedestal remains at low collisionality and is limited primarily by peeling modes, such that the attainable pedestal pressure is not reduced by positive perturbations in density [3]. H-modes have been shown to exhibit this property using strongly shaped plasmas at low collisionality on existing devices, confirming the predictive properties of EPED [16,17]. Examples of EPED predictions for the SPARC PRD, expressed in normalized pedestal pressure, are shown in Fig. 4, for three values of plasma triangularity about a baseline value of δ=0.49, and with the density scanned about the PRD target density. The influence of stronger shaping on pedestal performance is clearly illustrated.

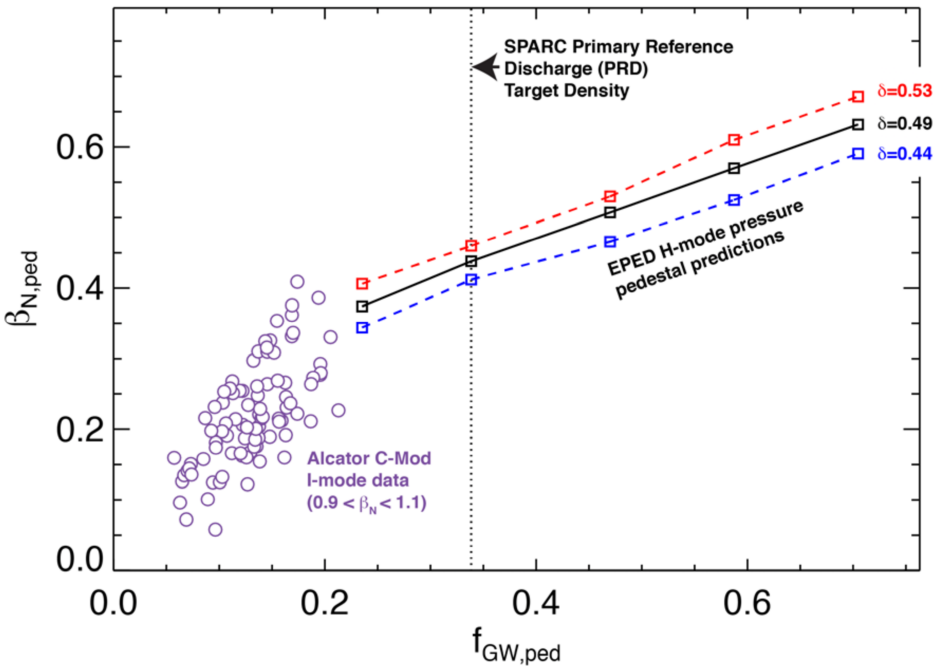

FIG. 4. Normalized pedestal pressure vs. normalized pedestal density, (1) predicted for the SPARC PRD H-mode (red, black, blue points) and (2) measured in Alcator C-Mod I-modes (purple circles). The mapping suggests potential for I-mode compatibility with SPARC target conditions and having pressure below limits imposed by peeling modes.

EPED predictions of the pedestal, given a set of operational plasma inputs (which include n_{ped}), form the key boundary conditions for H-mode simulations on SPARC. With the EPED boundary condition, core transport simulations have demonstrated satisfactory fusion gain (Q_{fus}~9) for the PRD discharge, roughly consistent with the outcome of POPCON analysis [2,7]. Simulations have also demonstrated a range of gains in H-modes, between 2 and 9, realized by introducing a pedestal penalty, i.e. a multiplier less than one applied to the EPED prediction [7]. A similar approach was used to generate the L-mode simulations in Table 1, and is expected to provide a framework for I-mode predictive transport and performance simulations.

Applying a penalty to the H-mode pedestal boundary condition remains the technique of choice for constraining I-mode core simulations, until improved predictive models are available for the I-mode pedestal. Since I-mode is not limited by peeling-ballooning modes in existing experiments [18], EPED and similar models cannot be used reliably, other than as an upper bound on the pedestal. Nonetheless, data from existing devices show promise for accessing the I-mode in SPARC and still maintaining a pedestal stable to peeling-ballooning modes. As an example, characteristic Alcator C-Mod I-mode data, taken from discharges having a similar global beta to that in the SPARC PRD, are overplotted as purple circles in Fig. 4. I-mode on C-Mod also operated in a density range that was consistent with accessing peeling modes in H-mode, albeit at reduced pedestal pressure. An example of this may be found in the access path for peeling limited H-modes, shown in [16]. Further mapping of non-dimensional I-mode parameters onto SPARC scenarios is the subject of ongoing work, as is work to more generally characterize the pedestal MHD in both I-modes and H-modes.

5. DISCUSSION

SPARC scenario development continues to rely on a mix of integrated transport modelling, empirical multi-machine scalings determining access to confinement modes, and reduced models of varied fidelity for the pedestal boundary condition. Using established empirical scalings for H-mode power thresholds and interpretive scalings of I-mode power threshold based on community findings, access to either regime appears feasible in SPARC, both in the PRD (12.2T, DT) and in scenarios at reduced field and in DD. H-mode avoidance may be a goal in early operation of SPARC. In this circumstance, operation with unfavourable drift direction would provide a clear path for testing I-mode access. The empirical and semi-empirical scalings above, coupled with high fidelity simulations of SPARC, will be expanded to better inform the early campaign planning for SPARC, specifically to identify regions of operating space that both defer H-mode access and promote I-mode access.

What are considered best estimates of L-H and L-I power thresholds may be conservative, based on L-mode transport simulations demonstrating large ratios of ion to electron heat flux in the edge plasma. If Q_i, rather than total power, is the critical parameter determining access to confinement mode transitions, then SPARC may be especially well suited to access these regimes at modest power levels. Whether this is generally true of burning plasma devices is a topic under active investigation.

H-mode pedestal predictions for SPARC are consistent with present day low collisionality H-modes having modestly strong shaping, and predicted normalized H-mode confinement also falls in line with existing machines. There is incomplete information on how to scale I-mode pedestals and confinement, although this is an active area of investigation across the devices that have obtained and studied the regime. Initial projections of I-mode pedestals from existing devices to SPARC show promise for utilizing the regime to achieve high energy confinement without large edge localized modes (ELMs), normally prevalent in H-modes.

ACKNOWLEDGEMENTS

This research was supported by Commonwealth Fusion Systems under RPP020. Alcator C-Mod data shown herein were generated under US Department of Energy Award DE-FC02-99ER54512.

REFERENCES

[1] CREELY, A., GREENWALD, M.J., BALLINGER, S.B. *et al.*, J. Plasma Physics, **86** 5 (2020) 865860502
[2] RODRIGUEZ-FERNANDEZ, P., CREELY, A.J., GREENWALD, M.J. *et al.*, Nucl. Fusion **62** (2022) 042003
[3] HUGHES, J.W., HOWARD, N.T., RODRIGUEZ-FERNANDEZ, P. *et al*., J. Plasma Physics, **86** 5 (2020) 865860504
[4] MARTIN, Y.R., TAKIZUKA, T., ITPA CDBM H-MODE THRESHOLD DATABASE WORKING GROUP, J. Physics Conf. **123** (2008) 012033
[5] RYTER, F., BARRERA ORTE, L., KURZAN, B. *et al*., Nucl. Fusion **54** (2014) 083003
[6] SCHMIDTMAYR, M., HUGHES, J.W., RYTER, F. *et al*., Nucl. Fusion **58** (2018) 056003
[7] RODRIGUEZ-FERNANDEZ, P., HOWARD, N.T., GREENWALD, M.J. *et al.*, J. Plasma Physics, **86** 5 (2020) 865860503
[8] WHYTE, D.G., HUBBARD, A.E., HUGHES, J.W. *et al.*, Nucl. Fusion **50** (2010)
[9] HUBBARD, A.E., BAEK, S.G., BRUNNER, D. *et al*., Nucl. Fusion **57** (2017) 126039
[10] HAPPEL, T., MANZ, P., RYTER, F. *et al*., Plasma Physics Control. Fusion **59** (2017) 014004
[11] RYTER, F., FISCHER, R., FUCHS, J.C. *et al*., Nucl. Fusion **57** (2017) 016004
[12] LIU, Y.J., LIU, Z.X., LIU, A.D. *et al.*, Nucl. Fusion **60** (2020) 082003
[13] RODRIGUEZ-FERNANDEZ, P., HOWARD, N.T., CANDY, J., Nucl. Fusion **62** (2022) 076036
[14] KAYE, S.M., ITER CONFINEMENT DATABASE WORKING GROUP, Nucl. Fusion **37** (1997) 1303
[15] SNYDER, P.B., GROEBNER, R.J., HUGHES, J.W. *et al.*, Nucl. Fusion **51** (2011) 103016
[16] HUGHES, J.W., SNYDER, P.B., REINKE, M.L. *et al.* Nucl. Fusion **58** (2018) 112003
[17] SNYDER, P.B., HUGHES, J.W., OSBORNE, T.H. *et al.* Nucl. Fusion **59** (2019) 086017
[18] WALK, J.R., HUGHES, J.W., HUBBARD, A.E. *et al.* Phys. Plasmas **21** (2014) 056103